Simulation of Continuous Solid-Phase Polymerization of Nylon 6,6. III. Simplified Model

K. Zhen Yao,[1] Kim B. McAuley,[1] E. Keith Marchildon[2]

[1]*Department of Chemical Engineering, Queen's University, Kingston, Ontario, Canada K7L 3N6*
[2]*DuPont Canada Inc., Research and Business Develop Center, Kingston, Ontario, Canada K7L 5A5*

Received 18 March 2002; accepted 11 January 2002

ABSTRACT: Solid-phase polymerization (SPP) reactors are used to increase the degree of polymerization (DP) during nylon 6,6 production. In previous articles, a reactor model with partial differential equations (PDEs) in time and two spatial dimensions was developed to describe dynamic changes in polymer property profiles (DP, temperature, and moisture content) over the height of the reactor and within the polymer particles. In the current article, a simplified model is developed by deriving appropriate expressions for heat- and mass-transfer coefficients and performing a lumped heat- and mass-transfer analysis. Using this approach, the radial dimension is removed from the PDEs, so that the effort required to solve the model equations is substantially reduced. Predictions of the complex and simplified models are compared through simulation of two different start-up processes. Good agreement between simplified and complex models is obtained, indicating that the simplified model can be used in place of the complex model if the polymer properties profiles within individual particles are not of particular concern to the model user. © 2003 Wiley Periodicals, Inc. J Appl Polym Sci 89: 3701–3712, 2003

Key words: nylon; solid-state polymerization; modeling; diffusion

INTRODUCTION

Solid-phase polymerization (SPP) processes are widely used in the commercial production of nylon and polyester. In these processes, polymer particles with moderate molecular weight are heated to a temperature between their glass transition temperature and melting temperature and polymerized to higher molecular weights.[1–9] In our previous work,[10,11] a reactor model was developed to describe the dynamics of a continuous SPP process for nylon 6,6 in a moving bed reactor. Temperature, moisture-content, and particle-property profiles over the height of the bed and within the polymer particles were determined at different reaction times under various operating conditions. A schematic diagram of the reactor system is shown in Figure 1. In a typical SPP process, semicrystalline polymer particles of a relatively low degree of polymerization (DP) are fed to the top of the vessel and removed from the bottom, while a countercurrent moist nitrogen stream is introduced at the bottom (Fig. 1).[9]

The previous reactor model consists of a set of PDEs in time and two spatial dimensions, z and r (Table I), where z is the vertical distance from the bottom of the SPP vessel and r is the radial distance from the center of each particle. The model equations were solved using VLUGR2,[12] an adaptive-grid finite-difference solver for time-dependent partial differential equations (PDEs) in two spatial dimensions. Solving these PDEs required considerable computational effort. For example, it took 1.5 h of CPU time on a personal computer with a P3 600-MHz CPU to simulate 17.5 h of reactor operation. The model can be simplified by performing a lumped heat- and-mass-transfer analysis, incorporating appropriate heat- and mass-transfer coefficients to predict the rates of heat and moisture transfer within the particles. Using this approach, average (rather than radially dependent) particle properties are considered at various heights and times in the reactor, resulting in a set of one-dimensional PDEs in the vertical direction, z, and time. In this work, the lumped model is developed and its predictions are compared with those of the former complex model.

Model development

The benefit of using a lumped model, which does not explicitly account for concentration and temperature gradients within the polymer particles, is that the dimension r is removed from the PDEs, so that the effort required to solve the model equations is substantially reduced. The lumped model equations are listed in Table II. It can be seen that PDEs (8) and (9) from Table I, which do not have any dependence on r, can be used in the lumped model without any changes. All the other PDEs require some modification because the version in Table I describes properties that

Correspondence to: K. B. McAuley.

Journal of Applied Polymer Science, Vol. 89, 3701–3712 (2003)

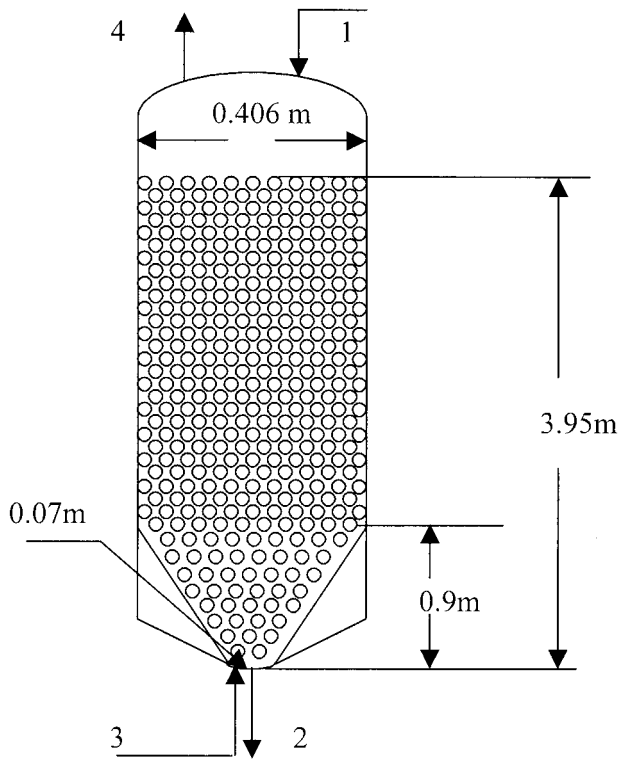

Figure 1 Nylon solid-state polymerizer: (1) polymer particles with relatively low DP; (2) polymer particles with higher DP; (3) gas inlet flow; (4) gas outlet flow.

change with respect to r or because they contain expressions involving the polymer properties at the particle surface (such as, p_{wR} and T_R, the vapor pressure of water and the temperature at the particle surface, respectively), which are not computed during the solution of the lumped model.

Changes in the average moisture content in the polymer phase ($\tilde{C}_w$) are governed by eq. (10). Here, the rate of overall moisture transport between the particles and gas phase is considered, rather than the local rate of moisture diffusion within the particles. k_o is an overall mass-transfer coefficient, which is related to a polymer-side mass-transfer coefficient (k_p) and gas-side mass-transfer coefficient (k_g) by

$$\frac{1}{k_o} = \frac{\mathbf{H}M_w}{k_p} + \frac{1}{k_g} \tag{28}$$

where **H** is a Henry's law constant and M_w is the molar mass of water. Expressions for k_p and k_g [eqs. (35) and (45)] are described in the next section of this article.

In eq. (10), $\tilde{p}_w$ is the vapor pressure of water that would be in equilibrium with the average polymer-phase moisture content, $\tilde{C}_w$:

$$\tilde{p}_w = \mathbf{H}\tilde{C}_w M_w \tag{29}$$

TABLE I
Model Equations for Nylon 6,6 Solid-phase Polymerization in a Continuous Moving Bed Reactor

$$\frac{\partial C_w}{\partial t} = D_{wp}\left[\frac{2}{r}\frac{\partial C_w}{\partial r} + \frac{\partial^2 C_w}{\partial r^2}\right] + r_p + \frac{\dot{m}_p}{\rho_p a_c(1-\varepsilon)}\frac{\partial C_w}{\partial z} + D_b\frac{\partial^2 C_w}{\partial z^2} \tag{1}$$

$$\frac{\partial C_c}{\partial t} = -r_p + \frac{\dot{m}_p}{\rho_p a_c(1-\varepsilon)}\frac{\partial C_c}{\partial z} + D_b\frac{\partial^2 C_c}{\partial z^2} \tag{2}$$

$$\frac{\partial C_a}{\partial t} = -r_p + \frac{\dot{m}_p}{\rho_p a_c(1-\varepsilon)}\frac{\partial C_a}{\partial z} + D_b\frac{\partial^2 C_a}{\partial z^2} \tag{3}$$

$$\frac{\partial C_l}{\partial t} = r_p + \frac{\dot{m}_p}{\rho_p a_c(1-\varepsilon)}\frac{\partial C_l}{\partial z} + D_b\frac{\partial^2 C_l}{\partial z^2} \tag{4}$$

$$\frac{\partial C_{wg}}{\partial t} = -\frac{\dot{m}_g}{\rho_g a_c \varepsilon}\frac{\partial C_{wg}}{\partial z} + D_{wg}\frac{\partial^2 C_{wg}}{\partial z^2} + \frac{D_{wg}}{a_c}\frac{da_c}{dz}\frac{\partial C_{wg}}{\partial z} + \frac{D_{wg}}{\varepsilon}\frac{\partial \varepsilon}{\partial z}\frac{\partial C_{wg}}{\partial z} + k_g(p_{wR} - p_{wg})\frac{3(1-\varepsilon)}{\varepsilon R} \tag{5}$$

$$\frac{\partial T}{\partial t} = -\frac{r_p\Delta\hat{H}_R}{C_p} + \frac{D_{wp}C_{pwl}}{C_p}\frac{\partial C_w}{\partial r}\frac{\partial T}{\partial r} + \frac{\kappa_p}{\rho_p C_p}\left[\frac{2}{r}\frac{\partial T}{\partial r} + \frac{\partial^2 T}{\partial r^2}\right] + \frac{\dot{m}_p}{\rho_p a_c(1-\varepsilon)}\frac{\partial T}{\partial z} + D_b\frac{\partial^2 T}{\partial z^2} \tag{6}$$

$$\frac{\partial T_g}{\partial t} = k_g(p_{wR} - p_{wg})\frac{3(1-\varepsilon)C_{pwv}(T_R - T_g)}{\varepsilon\rho_g C_{pg}R} + h_g(T_R - T_g)\frac{3(1-\varepsilon)}{\varepsilon\rho_g C_{pg}R} - \frac{\dot{m}_g}{\rho_g a_c\varepsilon}\frac{\partial T_g}{\partial z} + \kappa_g\frac{(1-\varepsilon)}{\varepsilon\rho_g C_{pg}}\frac{\partial^2 T_g}{\partial z^2} + \kappa_g\frac{(1-\varepsilon)}{\varepsilon a_c\rho_g C_{pg}}\frac{da_c}{dz}$$
$$- \frac{\partial T_g\kappa_g}{\partial z}\frac{\kappa_g}{\varepsilon\rho_g C_{pg}}\frac{\partial \varepsilon}{\partial z}\frac{\partial T_g}{\partial z} - h_w(T_g - T_w)\frac{2\nu\sqrt{a_\nu\pi}}{\varepsilon\rho_g C_{pg}a_c} \tag{7}$$

$$\frac{\partial \varepsilon}{\partial t} = \frac{\dot{m}_p}{\rho_p a_c(1-\varepsilon)}\frac{\partial \varepsilon}{\partial z} + D_b\frac{\partial^2 \varepsilon}{\partial z^2} \tag{8}$$

$$\frac{\partial R}{\partial t} = \frac{\dot{m}_p}{\rho_p a_c(1-\varepsilon)}\frac{\partial R}{\partial z} + D_b\frac{\partial^2 R}{\partial z^2} \tag{9}$$

TABLE II
Lumped Model Equations for Nylon 6,6 Solid-phase Polymerization in a Continuous Moving Bed Reactor

$$\frac{\partial \tilde{C}_w}{\partial t} = -3k_o \frac{(\tilde{p}_w - p_{\mathrm{wg}})}{R\rho_p} + r_p + \frac{\dot{m}_p}{(1-\varepsilon)a_c\rho_p}\frac{\partial \tilde{C}_w}{\partial z} + D_b \frac{\partial^2 \tilde{C}_w}{\partial z^2} \tag{10}$$

$$\frac{\partial \tilde{C}_c}{\partial t} = -r_p + \frac{\dot{m}_p}{\rho_p a_c(1-\varepsilon)}\frac{\partial \tilde{C}_c}{\partial z} + D_b \frac{\partial^2 \tilde{C}_c}{\partial z^2} \tag{11}$$

$$\frac{\partial \tilde{C}_a}{\partial t} = -r_p + \frac{\dot{m}_p}{\rho_p a_c(1-\varepsilon)}\frac{\partial \tilde{C}_a}{\partial z} + D_b \frac{\partial^2 \tilde{C}_a}{\partial z^2} \tag{12}$$

$$\frac{\partial \tilde{C}_l}{\partial t} = r_p + \frac{\dot{m}_p}{\rho_p a_c(1-\varepsilon)}\frac{\partial \tilde{C}_l}{\partial z} + D_b \frac{\partial^2 \tilde{C}_l}{\partial z^2} \tag{13}$$

$$\frac{\partial C_{\mathrm{wg}}}{\partial t} = -\frac{\dot{m}_g}{\varepsilon a_c \rho_g}\frac{\partial C_{\mathrm{wg}}}{\partial z} + D_{\mathrm{wg}}\frac{\partial^2 C_{\mathrm{wg}}}{\partial z^2} + \frac{D_{\mathrm{wg}}}{a_c}\frac{da_c}{dz}\frac{\partial C_{\mathrm{wg}}}{\partial z} + \frac{D_{\mathrm{wg}}}{\varepsilon}\frac{\partial \varepsilon}{\partial z}\frac{\partial C_{\mathrm{wg}}}{\partial z} + k_o(\tilde{p}_w - p_{\mathrm{wg}})\frac{3(1-\varepsilon)}{\varepsilon R} \tag{14}$$

$$\frac{\partial \tilde{T}}{\partial t} = -\frac{r_p \Delta \hat{H}_R}{C_p} - \Delta \hat{H}_{\mathrm{wv}}(\tilde{T})k_o \frac{3}{R\rho_p C_p}(\tilde{p}_w - p_{\mathrm{wg}}) + h_o \frac{3}{R\rho_p C_p}(T_g - \tilde{T}) + \frac{\dot{m}_p}{\rho_p(1-\varepsilon)a_c}\frac{\partial \tilde{T}}{\partial z} + D_b \frac{\partial^2 \tilde{T}}{\partial z^2} \tag{15}$$

$$\frac{\partial T_g}{\partial t} = k_o(\tilde{p}_w - p_{\mathrm{wg}})\frac{3(1-\varepsilon)C_{\mathrm{pwv}}(\tilde{T} - T_g)}{\varepsilon \rho_g C_{pg} R} + h_o(\tilde{T} - T_g)\frac{3(1-\varepsilon)}{\varepsilon \rho_g C_{\mathrm{pg}} R} - \frac{\dot{m}_g}{\varepsilon a_c \rho_g}\frac{\partial T_g}{\partial z} + \kappa_g \frac{(1-\varepsilon)}{\varepsilon \rho_g C_{\mathrm{pg}}}\frac{\partial^2 T_g}{\partial z^2} + \kappa_g \frac{(1-\varepsilon)}{\varepsilon a_c \rho_g C_{\mathrm{pg}}}\frac{da_c}{dz}\frac{\partial T_g}{\partial z} - \frac{\kappa_g}{\varepsilon \rho_g C_{\mathrm{pg}}}\frac{\partial \varepsilon}{\partial z}\frac{\partial T_g}{\partial z} - h_w(T_g - T_w)\frac{2\nu\sqrt{a_v \pi}}{\varepsilon a_c \rho_g C_{\mathrm{pg}}} \tag{16}$$

$$\frac{\partial \varepsilon}{\partial t} = \frac{\dot{m}_p}{\rho_p a_c(1-\varepsilon)}\frac{\partial \varepsilon}{\partial z} + D_b \frac{\partial^2 \varepsilon}{\partial z^2} \tag{17}$$

$$\frac{\partial R}{\partial t} = \frac{\dot{m}_p}{\rho_p a_c(1-\varepsilon)}\frac{\partial R}{\partial z} + D_b \frac{\partial^2 R}{\partial z^2} \tag{18}$$

p_{wg} is the vapor pressure of water in the gas phase, which can be determined using the ideal gas law:

$$p_{\mathrm{wg}} = C_{\mathrm{wg}} \Re T_g \tag{30}$$

In this work, we assume that the particles flow downward through the bed, at a mass flow rate $\dot{m}_p$, in a nearly ideal plug flow. A modification of the ideal reactor assumption is made by imposing a small amount of axial dispersion, $D_b[(\partial^2 C_w)/(\partial z^2)]$. For ideal plug flow, D_b is zero.

r_p, in eq. (10), is the rate of water generation (and polymerization), which is given by

$$r_p = k(C_c^2 C_a - C_w C_l C_c / K_{\mathrm{eq}}) \tag{31}$$

k, the kinetic rate constant for nylon polymerization, depends on the moisture concentration as well as on the temperature. In this work, the kinetics proposed by Mallon and Ray[13] were used.

$\tilde{C}_c$, $\tilde{C}_a$, and $\tilde{C}_l$ are average concentrations of carboxyl ends, amine ends, and amide links in the polymer phase, respectively. Changes in $\tilde{C}_c$, $\tilde{C}_a$, and $\tilde{C}_l$ with the vertical position and time are described by eqs. (11)–(13). Since the material balances on carboxyl ends, amine ends, and amide links in a complex model do not explicitly contain radial gradients, eqs. (11)–(13) are identical to eqs. (2)–(4) in Table I, except that radially dependent concentrations C_c, C_a, and C_l are replaced by the corresponding average concentrations, $\tilde{C}_c$, $\tilde{C}_a$, and $\tilde{C}_l$. All concentrations in the polymer phase are expressed in moles per unit mass of polymer.

The moisture concentration in the gas phase, C_{wg}, is governed by eq. (14). Compared with eq. (5) in Table I, the only difference is in the calculation of the moisture transport rate from the particles into the gas phase. Since the moisture concentration at the surface of the particle is unknown in the lumped model, an overall mass-transfer coefficient and driving force are used instead of the gas-side coefficient and driving force used in the complex model.

The average polymer-phase temperature is described by eq. (15). h_o is an overall heat-transfer coefficient, which is related to a polymer-side coefficient (h_p) and a gas-side coefficient (h_g) by

$$\frac{1}{h_o} = \frac{1}{h_p} + \frac{1}{h_g} \tag{32}$$

The calculation of h_p and h_g are discussed in the next section.

$\Delta\hat{H}_R$ is the enthalpy of reaction. Since nylon 6,6 crystallizes rapidly during the particle-formation stage, there is little change in the degree of crystallinity of the polymer within the SPP vessel. As a result, any heat effects associated with crystallization of an amorphous polymer are neglected. The enthalpy of vaporization of water evaporating from the surface of the particles, $\Delta\hat{H}_{wv}$, was accounted for by using a boundary condition in the complex model, but appears directly in eq. (15) in the lumped model.

Changes in the gas-phase temperature are governed by eq. (16). Gas-side heat- and mass-transfer coefficients and driving forces are replaced by the overall coefficients and driving forces, since the condition of the polymer at the particle surface is not known in the lumped model.

The voidage (ε) and the volume-average radius (R) of particles will change with the time and the vertical position if the bulk density and size of the polymer particles in the feed stream vary with the time. These changes are still described by eqs. (8) and (9).

A set of boundary conditions (BCs) is required to solve the model equations. One complication is that some boundary conditions must be specified at the top surface of the polymer bed ($z = H$). As the polymer inflow rate, outflow rate, and voidage change with the time, the bed height, H, changes according to

$$\frac{dH}{dt} = \frac{\dot{m}_{\text{pin}}}{a_{\text{cH}}\rho_p(1-\varepsilon_{\text{in}})} - \frac{\dot{m}_{p0}}{a_{\text{cH}}\rho_p(1-\varepsilon_0)} \tag{33}$$

where a_{cH} is the cross-sectional area of the vessel at the top surface of the bed.

Rather than attempting to solve a complex moving-boundary problem, it is much simpler to transform the PDEs in Table II using a dimensionless vertical coordinate, w, where $w = z/H$, so that w always has the value 1 at the top of the bed, even though the bed height changes over time.[11] A set of transformed PDEs and their boundary conditions are given in Table III(a,b). When situations involving step changes in inlet feed conditions are simulated, an additional transformation to track the movement of the steep front can also be applied to improve simulation accuracy and reduce the computational time.[11]

Calculation of heat- and mass-transfer coefficients

The overall heat- and mass-transfer coefficients required for the simplified model depend on the polymer-side and gas-side coefficients [eqs. (28) and (32)]. The gas-side coefficients can be determined from the Colburn j_H factor, which is empirically related to the Reynold's number (N_{Re}) for the gas moving through the bed[14]:

For heat transfer:

$$\begin{aligned} h_g &= \frac{j_H C_{\text{pg}}\dot{m}_g}{a_c}\left(\frac{\mu_g C_{\text{pg}}}{\kappa_g}\right)_f^{-2/3} \\ j_H &= \begin{cases} 0.91N_{\text{Re}}^{-0.51} & N_{\text{Re}} < 50 \\ 0.61N_{\text{Re}}^{-0.41} & N_{\text{Re}} > 50 \end{cases} \\ h_w &= \frac{0.813\kappa_g}{e^{6d_p/D}D}\left(\frac{d_p\dot{m}_g}{a_v\mu_g}\right)^{0.9} \end{aligned} \tag{34}$$

For mass transfer:

$$\begin{aligned} k_g &= \frac{j_D\dot{m}_g}{p_{N_2m}a_cM_g}\left(\frac{\mu_g}{\rho_g D_{wg}}\right)_f^{-2/3} \\ j_D &= \begin{cases} 0.91N_{\text{Re}}^{-0.51} & N_{\text{Re}} < 50 \\ 0.61N_{\text{Re}}^{-0.41} & N_{\text{Re}} > 50 \end{cases} \\ p_{N_2m} &= \frac{p_{N^2R} - p_{N_2g}}{\ln\left(\dfrac{p_{N_2R}}{p_{N_2g}}\right)} \\ p_{N_2R} &= P - p_{\text{wR}}, \qquad p_{N_2g} = y_{N_2}P \end{aligned} \tag{35}$$

Here, N_{Re} is given by

$$N_{\text{Re}} = \frac{\dot{m}_g R}{3(1-\varepsilon)a_c\mu_g}$$

The subscript f in eqs. (32) and (33) indicates that the Prandtl number and the Schmidt number should be determined at the film temperature, $T_f = \frac{1}{2}(T_g + T_R)$, between the bulk gas-phase temperature and the surface temperature of the particles.

The calculation of the polymer-side heat-transfer coefficient is more complicated: Carslaw and Jaeger[15] solved the problem of the conduction of heat from a sphere (with uniform initial temperature, T_{in}) to its outer surface, which is held at a constant temperature, T_R. They showed that the average temperature within the sphere at any time is given by the analytical expression

$$\tilde{T} = T_R - \frac{6(T_R - T_{in})}{\pi^2}\sum_{n=1}^{\infty}\frac{1}{n^2}e^{-\alpha n^2\pi^2 t/R^2} \tag{36}$$

where $\alpha = \kappa_p/\rho_p C_p$ is the thermal diffusivity of the sphere. Imagine that the sphere is initially hotter than the surface temperature, T_R; then, the rate of heat transfer from the sphere to its outer edge can be expressed as

$$-\frac{4}{3}\pi R^3\rho_p C_p\frac{d\tilde{T}}{dt} = 4\pi R^2 h_p(\tilde{T} - T_R) \tag{37}$$

where h_p is a polymer-side heat-transfer coefficient.

Differentiating the expression for $\tilde{T}$ in eq. (36) gives

TABLE III
Transformed Lumped Model Equations for Nylon 6,6 Solid-phase Polymerization in a Continuous Moving Bed Reactor

(a)

$$\frac{\partial \tilde{C}_w}{\partial t} = -3k_o\frac{(\tilde{p}_w - p_{\mathrm{wg}})}{R\rho_p} + r_p + \left[\frac{\dot{m}_p}{H(1-\varepsilon)a_c\rho_p} + \frac{w}{H}\frac{dH}{dt}\right]\frac{\partial \tilde{C}_w}{\partial w} + D_b\frac{\partial^2 \tilde{C}_w}{\partial w^2} \tag{19a}$$

$$\frac{\partial \tilde{C}_c}{\partial t} = -r_p + \left[\frac{\dot{m}_p}{H\rho_p a_c(1-\varepsilon)} + \frac{w}{H}\frac{dH}{dt}\right]\frac{\partial \tilde{C}_c}{\partial w} + D_b\frac{\partial^2 \tilde{C}_c}{\partial w^2} \tag{20a}$$

$$\frac{\partial \tilde{C}_a}{\partial t} = -r_p + \left[\frac{\dot{m}_p}{H\rho_p a_c(1-\varepsilon)} + \frac{w}{H}\frac{dH}{dt}\right]\frac{\partial \tilde{C}_a}{\partial w} + D_b\frac{\partial^2 \tilde{C}_a}{\partial w^2} \tag{21a}$$

$$\frac{\partial \tilde{C}_l}{\partial t} = r_p + \left[\frac{\dot{m}_p}{H\rho_p a_c(1-\varepsilon)} + \frac{w}{H}\frac{dH}{dt}\right]\frac{\partial \tilde{C}_l}{\partial w} + D_b\frac{\partial^2 \tilde{C}_l}{\partial w^2} \tag{22a}$$

$$\frac{\partial C_{\mathrm{wg}}}{\partial t} = \left(-\frac{\dot{m}_g}{H\varepsilon a_c\rho_g} + \frac{w}{H}\frac{dH}{dt}\right)\frac{\partial C_{\mathrm{wg}}}{\partial w} + \frac{D_{\mathrm{wg}}}{H^2}\frac{\partial^2 C_{\mathrm{wg}}}{\partial w^2} + \frac{D_{\mathrm{wg}}}{Ha_c}\frac{da_c}{dz}\frac{\partial C_{\mathrm{wg}}}{\partial w} + \frac{D_{\mathrm{wg}}}{H^2\varepsilon}\frac{\partial \varepsilon}{\partial w}\frac{\partial C_{\mathrm{wg}}}{\partial w} + k_o(\tilde{p}_w - p_{\mathrm{wg}})\frac{3(1-\varepsilon)}{\varepsilon R} \tag{23a}$$

$$\frac{\partial \tilde{T}}{\partial t} = \frac{r_p\Delta\hat{H}_R}{C_p} - \Delta\hat{H}_{\mathrm{wv}}(\tilde{T})k_o\frac{3}{R\rho_p C_p}(\tilde{p}_w - p_{\mathrm{wg}}) + h_o\frac{3}{R\rho_p C_p}(T_g - \tilde{T}) + \left[\frac{\dot{m}_p}{H\rho_p(1-\varepsilon)a_c} + \frac{w}{H}\frac{dH}{dt}\right]\frac{\partial \tilde{T}}{\partial w} + D_b\frac{\partial^2 \tilde{T}}{\partial w^2} \tag{24a}$$

$$\frac{\partial T_g}{\partial t} = k_o(\tilde{p}_w - p_{\mathrm{wg}})\frac{3(1-\varepsilon)C_{\mathrm{pwv}}(\tilde{T} - T_g)}{\varepsilon\rho_g C_{\mathrm{pg}}R} + h_o(\tilde{T} - T_g)\frac{3(1-\varepsilon)}{\varepsilon\rho_g C_{\mathrm{pg}}R} + \left(\frac{-\dot{m}_g}{H\varepsilon a_c\rho_g} + \frac{w}{H}\frac{dH}{dt}\right)\frac{\partial T_g}{\partial w} + \kappa_g\frac{(1-\varepsilon)}{H^2\varepsilon\rho_g C_{\mathrm{pg}}}\frac{\partial^2 T_g}{\partial w^2}$$
$$+ \kappa_g\frac{(1-\varepsilon)}{H\varepsilon a_c\rho_g C_{\mathrm{pg}}}\frac{da_c}{dz} - \frac{\kappa_g}{H^2\varepsilon\rho_g C_{\mathrm{pg}}}\frac{\partial \varepsilon}{\partial w}\frac{\partial T_g}{\partial w} - h_w(T_g - T_w)\frac{2\nu\sqrt{a_v\pi}}{\varepsilon a_c\rho_g C_{\mathrm{pg}}} \tag{25a}$$

$$\frac{\partial \varepsilon}{\partial t} = \left(\frac{\dot{m}_p}{H\rho_p a_c(1-\varepsilon)} + \frac{w}{H}\frac{dH}{dt}\right)\frac{\partial \varepsilon}{\partial w} + D_b\frac{\partial^2 \varepsilon}{\partial w^2} \tag{26a}$$

$$\frac{\partial R}{\partial t} = \left(\frac{\dot{m}_p}{H\rho_p a_c(1-\varepsilon)} + \frac{w}{H}\frac{dH}{dt}\right)\frac{\partial R}{\partial w} + D_b\frac{\partial^2 R}{\partial w^2} \tag{27a}$$

(b) Boundary conditions for the equations in (a)

$$\tilde{C}_w|_{w=1} = C_{\mathrm{win}} \tag{19b}$$

$$\tilde{C}_a|_{w=1} = C_{\mathrm{ain}} \tag{20b}$$

$$\tilde{C}_c|_{w=1} = C_{\mathrm{cin}} \tag{21b}$$

$$\tilde{C}_l|_{w=1} = C_{\mathrm{lin}} \tag{22b}$$

$$\frac{\dot{m}_{g0}y_{w0}}{M_0} = \frac{\dot{m}_{g0}C_{\mathrm{wg}}|_{w=0^+}}{\rho_g} + \frac{D_{\mathrm{wg}}\varepsilon a_c}{H}\frac{\partial C_w}{\partial w}\bigg|_{w=0^+}, \qquad \frac{\partial C_z}{\partial w}\bigg|_{w=1} = 0 \tag{23b}$$

$$\tilde{T}|_{w=1} = T_{\mathrm{in}} \tag{24b}$$

$$\dot{m}_{g0}C_{\mathrm{pg}}T_{g0} = \dot{m}_{g0}C_{\mathrm{pg}}T_g|_{w=0^+} + \frac{\kappa_g\varepsilon a_c}{H}\frac{\partial T_g}{\partial w}\bigg|_{w=0^+}, \qquad \frac{\partial T_g}{\partial w}\bigg|_{w=1} = 0 \tag{25b}$$

$$\varepsilon|_{w=1} = \varepsilon_{\mathrm{in}} \tag{26b}$$

$$R|_{w=1} = R_{\mathrm{in}} \tag{27b}$$

$$\frac{d\tilde{T}}{dt} = \frac{6(T_R - T_{in})\alpha}{R^2} \sum_{n=1}^{\infty} e^{-\alpha n^2 \pi^2 t/R^2} \tag{38}$$

Substituting for $d\tilde{T}/dt$ and solving eq. (37) for the polymer-side heat-transfer coefficient gives

$$h_p = 2\kappa_p \frac{(T_{in} - T_R)}{R(\tilde{T} - T_R)} \sum_{n=1}^{\infty} e^{-\alpha n^2 \pi^2 t/R^2} \tag{39}$$

Rearranging eq. (36) gives

$$\frac{T_{in} - T_R}{\tilde{T} - T_R} = \frac{\pi^2}{6 \sum_{n=1}^{\infty} \frac{1}{n^2} e^{-\alpha n^2 \pi^2 t/R^2}} \tag{40}$$

Equation (40) can be substituted into the expression for h_p in eq. (39) to give

$$h_p = \frac{\kappa_p \pi^2 \sum_{n=1}^{\infty} e^{-\alpha n^2 \pi^2 t/R^2}}{3R \sum_{n=1}^{\infty} \frac{1}{n^2} e^{-\alpha n^2 \pi^2 t/R^2}} \tag{41}$$

Equation (41) allows us to calculate a polymer-side heat-transfer coefficient to describe the cooling of spherical nylon pellets from an initial uniform temperature. Note that the heat-transfer coefficient depends on the pellet size and its thermal properties and that the heat-transfer coefficient changes over time. As $t \to 0$, $h_p \to \infty$ (due to the infinite initial temperature gradient at $r = R$), and as $t \to \infty$, $h_p \to (\kappa_p \pi^2)/(3R)$.

It would be convenient to use a representative time-invariant value for the heat-transfer coefficient in the SPP model. If we assume, for a moment, that h_p is independent of time, then eq. (37) can be solved analytically to give

$$\tilde{T} = T_R + (T_{\text{in}} - T_R) e^{-3h_p t/\rho_p C_p R} \tag{42}$$

This equation can be compared with the true solution given by eq. (36) for different constant values of h_p. This was done for a typical simulation, where spherical nylon pellets with $R = 0.0016$ m were heated from an initial temperature of 25°C by holding their outer-edge temperature at 190°C. The results are shown in Figure 2. As expected, using the value of h_p that is approached as $t \to \infty$ in eq. (42) gives a temperature rise in the particle that is too slow. However, choosing 1.5 times the infinite-time heat-transfer coefficient gives a reasonable temperature-rise prediction for the pellet. Using this fixed value for the heat-transfer coefficient causes the average pellet temperature to be underpredicted at times below about 2 s and slightly overpredicted at times greater than 2 s. Other values for the heat-transfer coefficients, ranging between 1.4 and 1.6 times the infinite-time heat-transfer coefficient, were used to simulate the behavior shown in Figure 2. All give reasonable predictions, indicating that the model predictions are not particularly sensitive to the recommended value of 1.5.

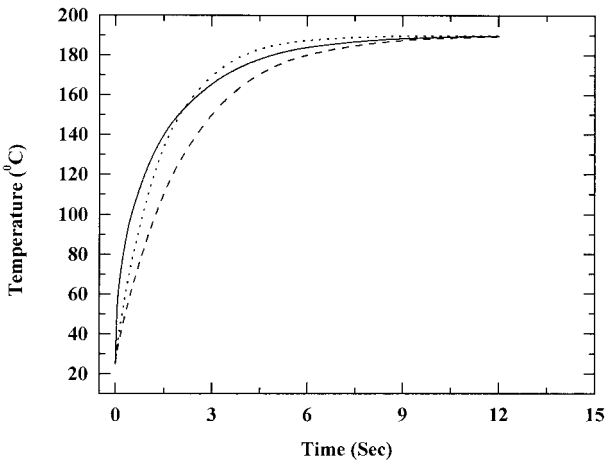

Figure 2 Heating of nylon 6,6 sphere: (—) exact solution; (–) terminal h_p; (· · ·) 1.5 terminal h_p.

By analogy to eq. (36), the average moisture concentration in the polymer pellets (with an initial uniform moisture concentration of C_{win} mol/unit mass) can be determined from

$$\tilde{C}_w = C_{\text{wR}} - \frac{6(C_{\text{wR}} - C_{\text{win}})}{\pi^2} \sum_{n=1}^{\infty} \frac{1}{n^2} e^{-D_{\text{wp}} n^2 \pi^2 t/R^2} \tag{43}$$

if the moisture concentration at the outer edge of the pellets is held at C_{wR}. D_{wp} is the diffusivity of water in the nylon pellets. Imagine that the moisture content of the spherical pellet is initially higher than is the moisture content in the polymer at the pellet surface. The rate of moisture transport from the sphere to its outer edge is given by

$$-\frac{4}{3}\pi R^3 \rho_p \frac{d\tilde{C}_w}{dt} = 4\pi R^2 k_p (\tilde{C}_w - C_{\text{wR}}) \tag{44}$$

Using eqs. (43) and (44) and a method analogous the derivation of eq. (41), a polymer-side mass-transfer coefficient can be obtained:

$$k_p = \frac{D_{\text{wp}} \rho_p \pi^2 \sum_{n=1}^{\infty} e^{-D_{\text{wp}} n^2 \pi^2 t/R^2}}{3R \sum_{n=1}^{\infty} \frac{1}{n^2} e^{-D_{\text{wp}} n^2 \pi^2 t/R^2}} \tag{45}$$

As expected, this polymer-side mass-transfer coefficient depends on the diffusivity and radius of the

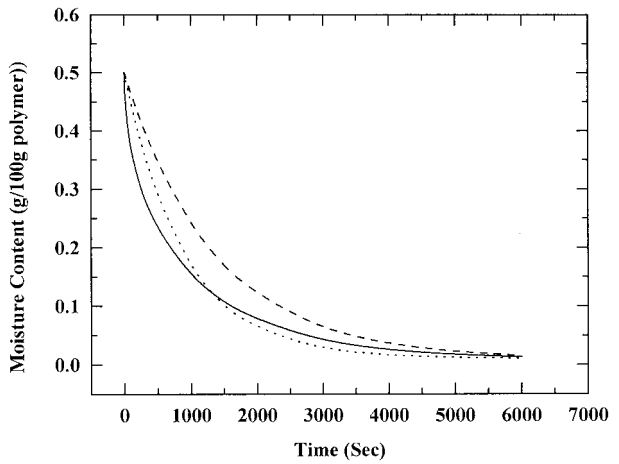

Figure 3 Drying of nylon 6,6 sphere: (—) exact solution; (–) terminal k_p; (· · ·) 1.5 terminal k_p.

polymer pellet. k_p also changes with time. When $t \rightarrow 0$, $k_p \rightarrow \infty$, and when $t \rightarrow \infty$, $k_p \rightarrow (D_{\mathrm{wp}}\rho_p\pi^2)/(3R)$.

If we neglect the dependence of k_p on time, then eq. (44) can be solved to get the following expression for the average moisture concentration within the pellet:

$$\tilde{C}_w = C_{\mathrm{wR}} + (C_{\mathrm{win}} - C_{\mathrm{wR}})e^{-3k_pt/(R\rho_p)} \qquad (46)$$

As shown in Figure 3, this equation can be compared with the true solution given in eq. (43) for different constant values of k_p. This was done for a typical simulation wherein spherical nylon pellets with $R = 0.0016$ m were dried from an initial uniform moisture concentration of 0.5 g/100 g polymer by holding the moisture content of their surface at a constant concentration of 0.01 g moisture per 100 g polymer. As expected, using $k_p = (D_{\mathrm{wp}}\rho_p\pi^2)/(3\mathrm{R})$, the value of the polymer-side mass-transfer coefficient at infinite time, in eq. (46) gives a drying rate that is too slow. A value that is 1.5 times the infinite-time mass-transfer coefficient, however, gives a reasonable approximation to the drying curve.

By comparing Figures 2 and 3, it can be found that mass transfer is much slower than is heat transfer. The time scale of thermal diffusion can be calculated as follows:

$$R^2/\alpha \approx 25 \text{ s}$$

where α is the thermal diffusivity. On the other hand, the mass-diffusion time (R^2/D_w) for the water in the particles is approximately 6 h. Therefore, it takes much more time for the moisture content to equilibrate within the polymer particles. Both heat- and mass-transfer rates become slower with an increasing particle size.

The particle-side heat- and mass-transfer coefficients that are used in this simplified SPP model were derived from analytical solutions for heat transfer in spherical particles under the restriction of constant boundary conditions. Fixed, rather than time-varying, values of the transfer constants were desired for use in the model equations, so time-invariant expressions were determined that approximate the behavior of the analytical solution. The SPP model that makes use of these heat- and mass-transfer constants permits time-varying, rather than fixed conditions at the particle boundary. To investigate the effects of these approximations, simulation results for the complex and lumped models are compared in the following sections.

RESULTS AND DISCUSSION

In our previous articles, the complex reactor models were solved using VLUGR2,[12] a numerical solver designed for time-dependent PDEs in two spatial dimensions. To compare the performance of complex and lumped models, without causing any influence due to different numerical solvers, VLUGR2 was also used to solve the lumped model equations in Table III. In this work, the PDE in one spatial dimension was solved as an artificial two-dimensional problem with only one node used in the artificial direction. This approach was suggested by Verwer.[16]

Simulation of reactor start-up

In previous articles,[10,11] the complex model was used to simulate two typical start-ups for nylon 6,6 SPP processes. In the first type of start-up, the reactor is initially filled with the particles that have the same properties as those entering the top of the vessel. In this simulation, the initial gas-phase temperature and gas-phase moisture fraction within the reactor were 25°C and 0.57 mol %, respectively. In the second process, particles are fed to a reactor initially containing

TABLE IV
Operating Conditions for the Simulation[9]

Residence time	3.5 h
Polymer mass flow rate	1.36 kg/min
Gas flow rate	47.2 L/s (at 25°C, 1 atm)
Temperature of inlet polymer	25°C
Temperature of inlet gas	190°C
Moisture of inlet polymer	0.3 wt %
Moisture fraction of inlet gas	0.57 mol %
Voidage of inlet polymer	0.45 (bulk density: 640 kg/m^3)
Particle radius	1.6 mm
Carboxyl ends in polymer inlet	0.06 mol/kg
Amine ends in polymer inlet	0.06 mol/kg
DP of inlet polymer	146

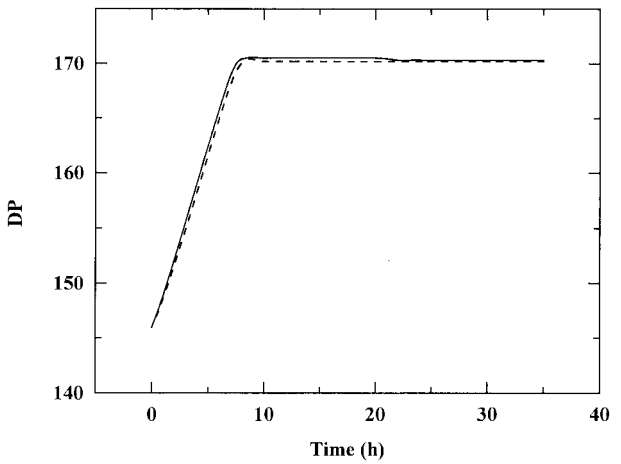

Figure 4 Dynamic evolution of DP at the outlet of SPP reactor (first start-up): (—) complex model; (–) lumped model.

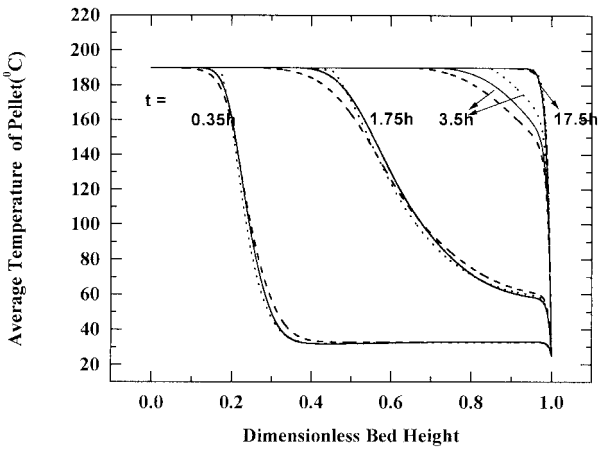

Figure 6 Profile of average temperature in the polymer phase at different reaction times (first start-up): (—) complex model; (–) lumped model; (· · ·) no mass-transfer resistance inside polymer particles.

only 6 kg of particles, giving a starting bed height of 0.2 m. The inflow rate is identical to that in the first start-up procedure, but there is no outflow of polymer from the reactor until the top surface of the bed reaches the desired level (H = 3.95 m). Thereafter, the polymer outflow is set equal to the inflow rate to maintain the top surface at a constant position. The other operating conditions for these start-up processes are shown in Table IV. The simulations were run on a personal computer with a P3 600-MHz CPU. When 200 nodes in the vertical direction were used, 1.5 h of CPU time were required to solve the complex model while the simplified model required only 15 min.

Simulation results for the first start-up procedure, using the complex and lumped models, are compared in Figures 4–10. The dynamic evolution of the DP and average polymer-phase moisture content at the outlet of the reactor are shown in Figures 4 and 5. The simulation results of the two models are very close to each other. At the steady state, the DP predicted by the complex model is 170.50, while the lumped model has the value of 170.18. The steady-state average moisture contents of the particles predicted by the two models are identical to three significant figures.

Figures 6 and 7 show the temperature profiles within the reactor at different reaction times. The temperature profiles predicted by both models are similar, with the complex model predicting a slightly steeper front within the bed. The expressions used in the two models to calculate the heat-transfer rate are as follows:

$$\text{Simplified model: } h_o(\tilde{T} - T_g) \tag{47}$$

$$\text{Complex model: } h_g(T_R - T_g) \tag{48}$$

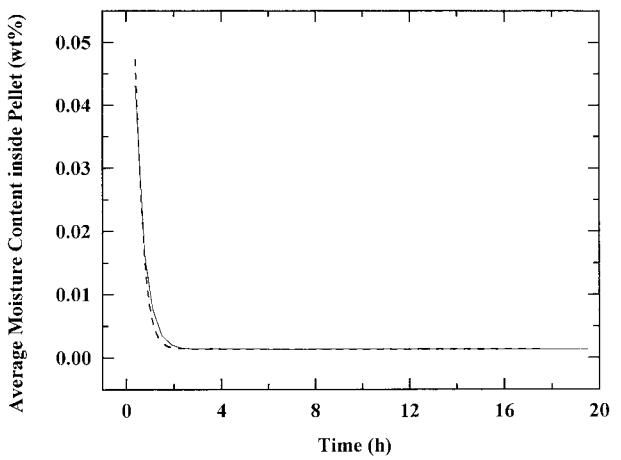

Figure 5 Dynamic evolution of average moisture content inside particle at the outlet of SPP reactor (first start-up): (—) complex model; (–) lumped model.

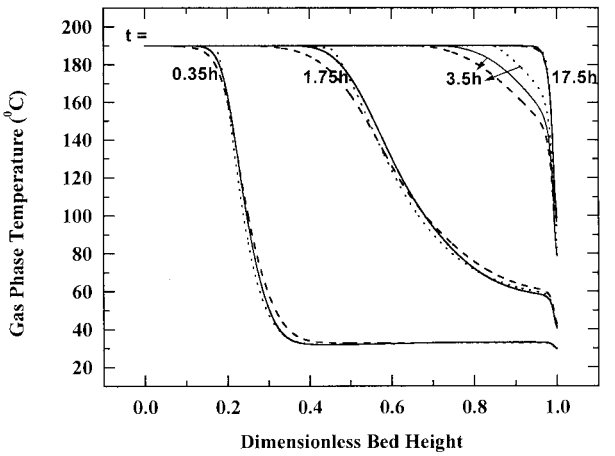

Figure 7 Profile of gas-phase temperature at different reaction times (first start-up): (—) complex model; (–) lumped model; (· · ·) no mass-transfer resistance inside polymer particles.

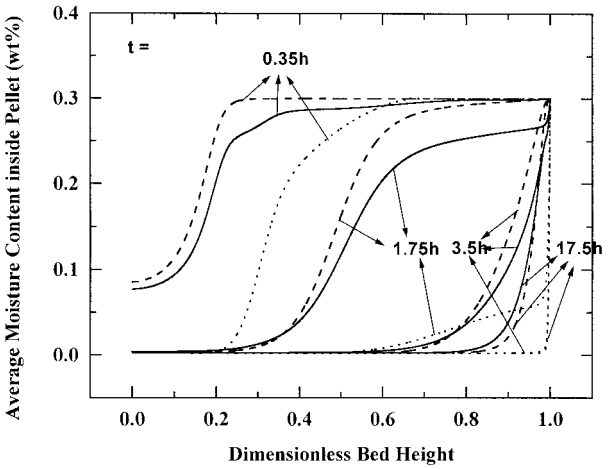

Figure 8 Profile of average moisture content in the polymer phase at different reaction times (first start-up): (—) complex model; (–) lumped model; (· · ·) no mass-transfer resistance inside polymer particles.

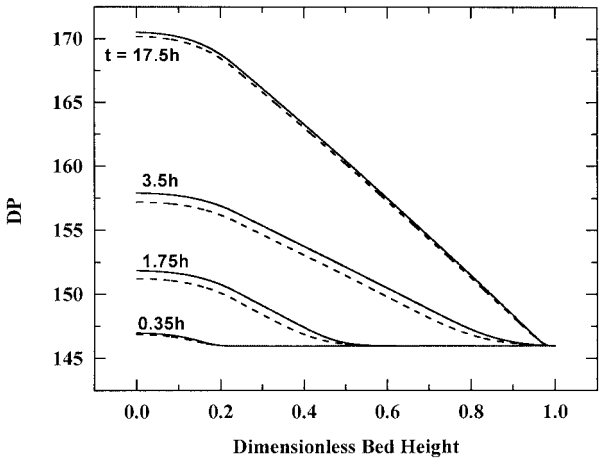

Figure 10 DP profile along the reactor at different reaction times (first start-up): (—) complex model; (–) lumped model.

As shown before, the thermal diffusion time (R^2/α) is about 25 s, which is very small compared to the 3.5-h residence time. Hence, there is almost no temperature gradient inside the particles after the first few seconds of residence time within the bed, and $\tilde{T}$, the average temperature, is very close to T_R, the temperature at the particle surface. The overall heat-transfer coefficient, h_o, is related to polymer-side coefficient, h_p, and gas-side coefficient, h_g, through eq. (30). One can expect that h_o is always smaller than is h_g, but that the difference between h_o and h_g is very small since h_p is much bigger than either h_o or h_g. To give an example, at the steady state, h_o, h_g, and h_p at position $z = 0.5$ are 142, 175, and 771 J m^{-2} K^{-1} s^{-1}, respectively. Therefore, the differences between heat-transfer rates calculated by eqs. (47) and (48) are small.

The simplified model accounts for heat-transfer resistance within particles using the particle-side heat-transfer coefficient. If we neglect the temperature gradients within the particles and assume a uniform temperature throughout the particles, that is, $h_p \to \infty$, then we get $h_o = h_g$. Simulation results obtained by neglecting the heat-transfer resistance inside particles are also shown in Figures 6 and 7 (dotted lines). It can be seen that, at the beginning of the process, the dotted lines are closer to the complex model predictions than are the simplified model predictions. As described in the previous section, as $t \to 0$, the true value of h_p is infinite immediately after a new temperature is imposed at the particle surface. A rapid flow of hot gas into the vessel causes a rapid rise in the particle surface temperature, so that the simplified model initially has a value of h_p that is too low. However, with increasing time, the true h_p becomes smaller and smaller, and it becomes inappropriate to neglect the

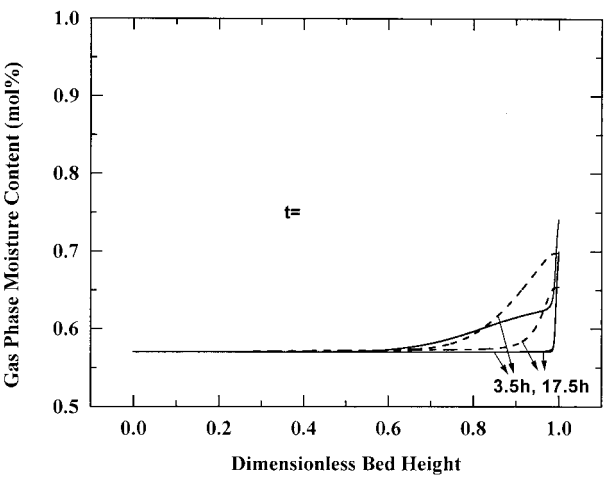

Figure 9 Profile of gas-phase moisture content along reactor at different reaction times (first start-up): (—) complex model; (–) lumped model.

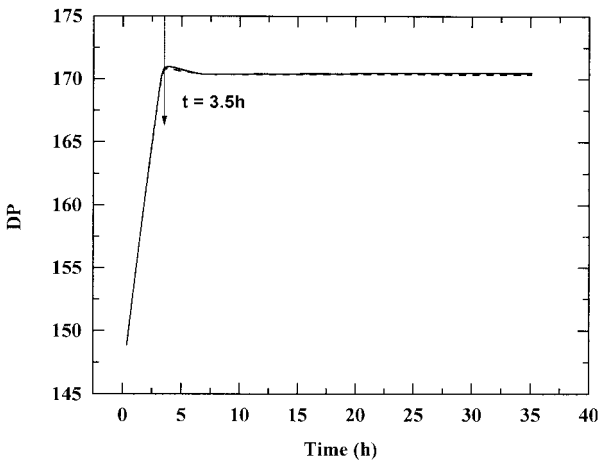

Figure 11 Dynamic evolution of DP at the outlet of SPP reactor (second start-up): (—) complex model; (–) lumped model.

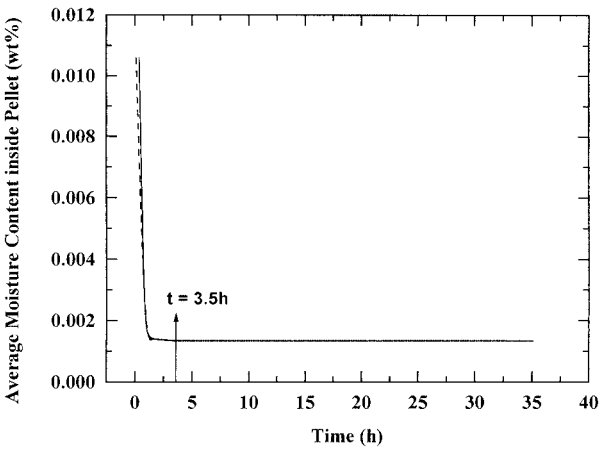

Figure 12 Dynamic evolution of average moisture content inside particle at the outlet of SPP reactor (second start-up): (—) complex model; (–) lumped model.

heat-transfer resistance. Therefore, in Figures 6 and 7, the dotted lines (no resistance) move away from the solid line (complex model) and become too steep. If the particle size is increased, the deviation between the dotted and solid lines becomes even larger, whereas the simplified model is able to automatically account for the effects of increasing particle size on heat-transfer rates.

The moisture profiles in both phases are presented in Figures 8 and 9. At the beginning of the start-up process, the moisture profiles predicted by the two models are quite different. The moisture content inside polymer particles obtained by the lumped model is higher than is the prediction of the complex model; in the gas phase, the complex model predicts a higher moisture concentration. However, at the steady state, the moisture content predicted by the lumped model is slightly lower in the polymer phase and higher in the gas phase, compared to the results of the complex model, and the differences are much smaller than at small times. This behavior could be anticipated because the true value of the polymer-side mass-transfer coefficient is very large at $t = 0$ and becomes smaller with increasing time. Therefore, in the simplified model, the constant value of k_p is too low initially and too high at the steady state.

The dotted lines in Figure 8 are obtained by neglecting mass-transfer resistances within the particles and replacing k_o with k_g to calculate the mass-transfer rate. It can be seen that, without considering polymer-side mass-transfer resistance, the moisture content profiles are very different from the results of the complex model.

Figure 10 shows the DP profiles inside the reactor. As expected, the DP profiles predicted by both models are very close to each other, with the simplified model predicting a slightly lower DP.

The simulation results for the second type of start-up, wherein the reactor bed starts at a very low level, are presented in Figures 11 and 12. As shown in these figures, the DP and polymer-phase moisture content at the reactor outlet are essentially at the final steady-state values before the polymer outlet stream is turned on. Therefore, no off-specification material is produced using this start-up policy. It can also be seen that the differences between the simplified model and the complex model are very small for this simulated start-up. Compared with the first start-up, there are few polymer particles initially inside the reactor, and these initial particles are quickly heated and dried. Under these conditions, it is reasonable to use time-independent polymer-side heat- and mass-transfer coefficients to describe the heat- and mass-transfer resistance within the particles and excellent agreement between the simplified and complex models is obtained.

CONCLUSIONS

The SPP reactor model developed in our previous work[10,11] was substantially simplified from a set of PDEs in time and two spatial dimensions to give an analogous set of PDEs in time and only one spatial dimension. The new model does not assume that the temperature and composition gradients within the polymer particles are negligible. Rather, novel analytical expressions for heat- and mass-transfer coefficients within the polymer particles were derived to account for heat conduction and moisture diffusion within the particles. These coefficients are able to explain the effects of particle size and the thermal and mass diffusivity of the polymer on rates of heat and moisture transport. Using these new particle-side heat- and mass-transfer coefficients, overall heat- and mass-transfer expressions were developed to model the reactor behavior. The resulting simplified model leads to substantial savings (by a factor of 10) in computational effort, with only a minor effect on the quality of the model predictions. We anticipate that the polymer-side heat- and mass-transfer coefficients developed in this work would be useful for other modelers who seek to simplify spherical-particle models in which heat conduction and mass diffusion inside particles are important.

Both complex and simplified models were used to simulate two types of start-up procedures for solid-phase nylon 6,6 production. These two models predicted consistent results for the average particle properties at the outlet of the reactor for both types of start-ups. The temperature profiles within the reactor predicted by the two models are very close to each other. The profiles of moisture content are different at the beginning of the process, but the difference becomes very small as the steady state is approached. It

is reasonable to replace the complex model with the simplified model if average particle properties, rather than polymer-property profiles within the particles, are the main concern of the model user. Even if more accurate results than those predicted by the lumped model are required by the model user, the lumped model would still be useful for preliminary trial-and-error simulation and scoping studies. The time-consuming complex model could then be reserved for obtaining final simulation results.

Using the model predictions, we have shown that the start-up process beginning with an empty reactor (second start-up process) can reach the steady state in only one residence time, compared with two residence times needed for the start-up process beginning with the reactor full of cold polymer particles (first start-up process). No off-specification product is obtained when the second start-up process is used.

NOMENCLATURE

a_c	cross-sectional area of reactor, m^2
C_a, C_c, C_l	concentration of amine ends, carboxyl ends, and amide links in particles, mol/kg
$\tilde{C}_c$, $\tilde{C}_a$, $\tilde{C}_l$	average concentration of amine ends, carboxyl ends, and amide links in particles, mol/kg
C_p, C_{pg}	heat capacity of polymer and moist nitrogen gas, J kg^{-1} K^{-1}
C_{pwl}, C_{pwv}	heat capacity of liquid water and water vapor, J mol^{-1} K^{-1}
C_w	concentration of water in polymer phase, mol/kg
$\tilde{C}_w$	average concentration of water in polymer phase, mol/kg
C_{wg}	concentration of water in gas phase, mol/L
C_{in}	inlet concentration of water in polymer phase, mol/kg
D_b	dispersion coefficient, m^2/s
d_p	particle diameter for the Ergun equation. For nonspherical particles, the diameter of a sphere with the same volume as the particle, m
D_{wg}, D_{wp}	diffusivity of water in gas phase and polymer phase, m^2/s
H	Henry's law coefficient, Pa
H	height of the top surface of the polymer bed, m
h_g	gas-side heat-transfer coefficients, J m^{-2} K^{-1} s^{-1}
h_o	overall heat-transfer coefficients, J m^{-2} K^{-1} s^{-1}
h_p	polymer-side heat-transfer coefficients, J m^{-2} K^{-1} s^{-1}
h_w	heat-transfer coefficients for heat transfer from gas phase to the wall of the bed, J m^{-2} K^{-1} s^{-1}
$\Delta\hat{H}_R$	heat of reaction, J/mol
$\Delta\hat{H}_{wv}$	eat of vaporization of water, J/mol
j_D	Colburn factor for gas-side mass-transfer correlations
j_H	Colburn factor for gas-side heat-transfer correlations
k	kinetic rate constant for polymerization reaction, kg^2 mol^{-2} s^{-1}
K_{eq}	equilibrium constant for polymerization
k_g	gas-side mass-transfer coefficients, mol m^{-2} atm s^{-1}
k_o	overall mass-transfer coefficients, mol m^{-2} atm s^{-1}
k_p	polymer-side mass-transfer coefficients, kg m^{-2} s^{-1}
$\dot{m}_g$, $\dot{m}_p$	mass flow rate of moisture gas and polymer, kg/s
M_w	molecular weight of water, kg/mol
N_{Re}	Reynolds number for moist N_2 gas
P	pressure inside the reactor, Pa
$\tilde{p}_w$	vapor pressure of water that is in equilibrium with the polymer with average polymer-phase moisture content, Pa
p_{wg}	partial pressure of water in the gas phase, Pa
p_{wR}	vapor pressure of water that is in equilibrium with the polymer with the surface moisture concentration, Pa
r	radial distance from the center of a spherical polymer particle, m
$\Re$	ideal gas constant, J mol^{-1} K^{-1}
r_p	rate of polymerization, mol kg^{-1} s^{-1}
t	time (s)
T	temperature of polymer, K
$\tilde{T}$	average temperature of polymer, K
T_g	temperature of gas phase, K
T_{in}	initial temperature, K
T_R	temperature at the particle surface, K
T_w	temperature of reactor wall, K
v	gas flow rate, m /s
w	dimensionless vertical coordinate, z/H
y_w	water mol fraction in the gas phase
z	height, measured from the bottom of the vessel, m

Greek letters

α	thermal diffusivity, m^2/s
ε	voidage
ϕ_S	sphericity of a nylon particle for use in the Ergun equation. The surface area of a sphere with the same volume as the particle, divided by the surface area of the particle
κ_g, κ_p	thermal conductivity of gas phase and polymer, W m^{-1} K^{-1}
μ_g	viscosity of gas phase, Pa s
ρ_g, ρ_p	density of gas phase and polymer, kg/m^3

References

1. Chipman, G. R.; Bockrath, R. E. U.S. Patent 4 008 206, 1977 (to Amoco).
2. Kaushik, A.; Gupta, S. K. J Appl Polym Sci 1992, 45, 507.
3. Mallon, F. K.; Ray, W. H. J Appl Polym. Sci 1998, 69, 1233.
4. Mallon, F. K.; Ray, W. H. J Appl Polym Sci 1998, 69, 1775.

5. Medellin, R. F.; Lopez, G. R.; Waldo, M. M. J Appl Polym Sci 2000, 75, 78.
6. Srinivasan, R.; Desai, P.; Abhiraman, A. S.; Knorr, R. S. J Appl Polym Sci 1994, 53, 1731.
7. Wendling, P. R. U.S. Patent 4 532 319, 1985 (to Goodyear).
8. Yao, Z.; Ray, W. H. AIChE J 2000, 47, 401.
9. Beaton, D. H. U.S. Patent 3821171, 1974 (to DuPont).
10. Yao, K. Z.; McAuley, K. B.; Berg, D.; Marchildon, E. K. Chem Eng Sci 2001, 56, 5327.
11. Yao, K. Z.; McAuley, K. B. Chem Eng Sci 2001, 56, 4801.
12. Blom, J. G.; Trompert, R. A.; Verwer J. G ACM Trans Math Software 1996, 22, 302.
13. Mallon, F. K.; Ray, W. H. J Appl Polym Sci 1998, 69, 1213.
14. Bird, R. B.; Stewart, W. E.; Lightfoot, E. N. Transport Phenomena; Wiley: New York, 1960; p 646.
15. Carslaw, H. S.; Jaeger, J. C. Conduction of Heat in Solids, 2nd ed.; Oxford University: Oxford, UK, 1959; p 233.
16. Verwer, J. G. Personal communication, 2000.